**Proceedings of the ASME 2009 International Design Engineering Technical Conferences & Computers and Information in Engineering Conference**
**IDETC/CIE 2009**
**August 30 - September 2, 2009, San Diego, California, USA**

# DETC2009-86638

# APPROXIMATE CLOSED-FORM SOLUTIONS FOR THE SHIFT MECHANICS OF RUBBER BELT VARIATORS

**Marco Cammalleri**
University of Palermo
Palermo, Italy

**Francesco Sorge**
University of Palermo
Palermo, Italy

## ABSTRACT

The mechanical behavior of V-belt variators during the speed ratio shift is different from the steady operation as a gross radial motion of the belt is superimposed to the circumferential motion. The theoretical analysis involves equilibrium equations similar to the steady case, but requires a re-formulation of the mass conservation condition making use of the Reynolds transport theorem. The mathematical model of the belt-pulley coupling implies the repeated numerical solution of a strongly non-linear differential system. Nevertheless, an attentive observation of the numerical diagrams suggests simple and useful closed-form approximations for the four possible working modes of any pulley, opening/closing, driver/driven, whose validity ranges over most practical cases. The present analysis focuses on the development of such simplified solutions, succeeding in an excellent matching with the numerical plots, and on the comparison of the theory with some experimental tests on a motorcycle variator, revealing a very good agreement.

## 1. INTRODUCTION

The operative condition of the continuously variable transmissions (CVT) for the vehicle application consists typically in a sequence of up-shift and down-shift phases of the speed ratio. The shift mechanics of V-belt variators differs from the steady operation due to the gross radial motion of the belt toward the inside/outside of the groove during the opening/closing of the half-pulleys.

In case of small power, as for example in motorcycles, a large use of rubber V-belt variators is now encountered since many years, while metal V-belt CVT's have just grown up widely in the automotive field in the last two decades.

The theory of the steady mechanics of rubber V-belt drives is now well-established [1-5], while the transient state has just begun to be studied by a rather limited number of researchers (e. g. see [6-11]), using different approaches for rubber belt variators and metal push-belt CVT's. In the last case, the pulley deformation is of the same order of magnitude of the belt or higher, so that the tension and penetration distributions appear quite different.

References [12-14] report some theoretical-experimental researches on the mechanics of rubber belt variators and on the devices employed to produce the belt forcing, usually by loading springs on the driven side, and to control the speed ratio, generally by centrifugal masses on the driver side, where proper tracks are created to get an efficient correlation between the engine speed and the speed ratio.

With the purpose of affording useful and practical tools for the drive design or inspection, the full mathematical model of reference [8] is here assumed as starting point for the construction of simple and practical approximate solutions. The theory of [8] was developed for a rubber belt and the final results involved the presence of adhesive or adhesive-like sub-regions inside the arc of contact, for the closing or opening pulleys respectively. Proofs of the existence or non-existence of these sub-regions were also given.

The solution of the full differential system is rather cumbersome, due to its strong non-linearity, and may be faced by Runge-Kutta routines, starting for example from the exit point of the wrap arc and reiterating the procedure by a sort of shooting technique until all the external boundary conditions are fulfilled (wrap arc, applied torque and axial thrust).

Nevertheless, examining a great deal of numerical diagrams, several particular features may be identified for the various cases, suggesting to develop simpler approximate solutions, valid throughout a wide range of practical cases. These closed-form approximations give an excellent fit and offer a very fine agreement with some experimental bench tests on rubber belt variators.

 

## 2. OUTLINE OF DRIVE SHIFT THEORY

The belt is considered as a one-dimensional continuous material flowing inside a stream tube of negligible cross-section formed by its own external surface, which is in motion in shift conditions. A dihedral control volume is considered and the Reynolds transport theorem is applied (see and refer to Fig. 1 for the notation).

Indicating with $x = (r_\infty - r)/r_\infty$ the dimensionless elastic penetration of the belt, scaled by the nominal radius $r_\infty$ (wrap radius for infinite transverse stiffness of the belt in the axial direction), and denoting the partial differentiation with respect to $\theta$ with primes, the geometrical condition $r' = -r\tan\chi$ becomes

$$x' = (1-x)\tan\chi \quad \rightarrow \quad x' \approx \tan\chi \qquad (1), (1_{abr.})$$

where its abridged form is reported on the right, neglecting $x \ll 1$. In the following, many equations with the numbering (…) will be rewritten on their right in an approximate form ($\dots_{abr.}$), neglecting small terms.

The total time derivative of the radial coordinate of a moving belt element is written as the sum of a local and a convective term, $dr/dt = \dot{r} + \dot{\theta}r'$, where dots indicate the partial differentiation with respect to the time $t$, and this relationship involves that $-v\sin\delta = \dot{r} - v\cos\delta\tan\chi$ by Fig. 1a. On the other hand, the triangle of velocities yields $v\cos\delta - \omega r - v\cdot\sin\delta\tan\gamma = 0$, where $\gamma$ is the sliding angle in the plane of rotation. Introducing the dimensionless shift speed $\rho = \dot{r}/(\omega\cdot r) \cong \dot{r}_\infty/(\omega\cdot r_\infty)$, which is presumed of the same order of magnitude of the strain variables of the belt ($x$, $\chi$ and the belt elongation $\varepsilon$, all of order ~ 1/1000 roughly), such geometrical-kinematical relationships can be combined into

$$\frac{v\cos\delta}{\omega\cdot r} = \frac{1-\rho\tan\gamma}{1-\tan\chi\tan\gamma} \qquad (2)$$

and it is observable that, if $\rho = \tan\chi$ and $1 - \tan\chi\tan\gamma \neq 0$, then $v\cos\delta = \omega r$ and $v\sin\delta = 0$, i. e. there is adhesion between the belt and the pulley. Therefore, $x' = (1-x)\rho \approx \rho$ along an adhesion region.

Combining the Eulerian and Lagrangian formulations of the mass conservation condition, accounting for Eqs. (1-2), introducing the belt elongation $\varepsilon = T/S_{//}$, equal to the ratio of the belt force $T$ to the longitudinal stiffness $S_{//}$, one may arrive, as in [8], at the equation

$$u' = (1+u)\left[\frac{\varepsilon'}{1+\varepsilon} + \tan\chi(1-\chi')\right] - \rho \quad \rightarrow \quad \rightarrow \quad u' \approx \varepsilon' + \tan\chi - \rho \qquad (3), (3_{abr.})$$

where $u$ is the dimensionless circumferential component of the sliding speed,

$$u = \frac{v_{slid.}}{\omega\cdot r}\sin\gamma = \frac{v\cos\delta}{\omega\cdot r} - 1 = \left(\frac{\tan\chi-\rho}{1-\tan\gamma\tan\chi}\right)\tan\gamma$$

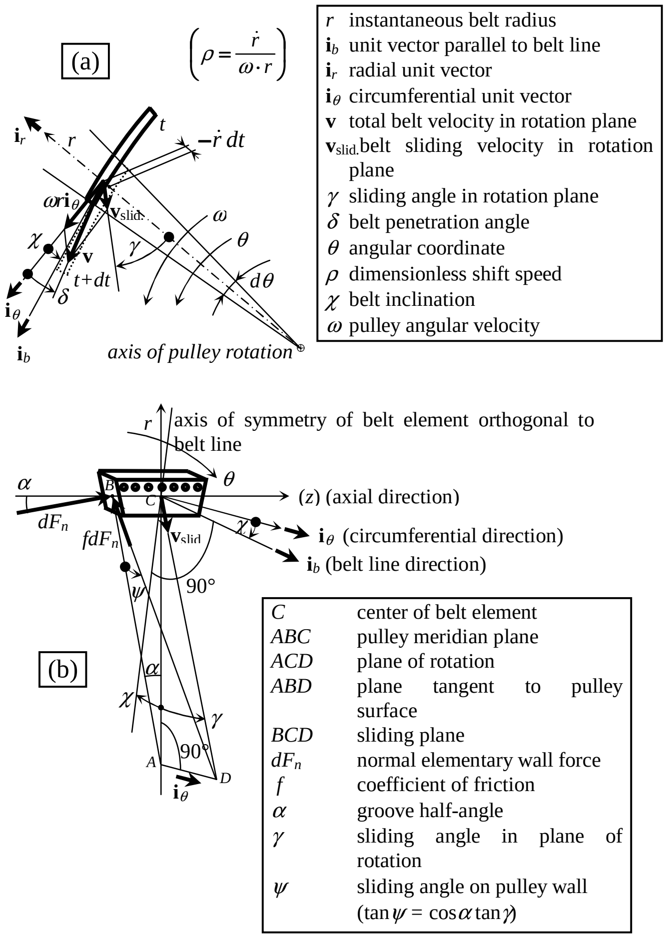


Figure 1. (a) Belt element passing through control volume, triangle of velocities. (b) Belt-pulley coupling

or inversely

$$\tan\gamma = \frac{u}{(1+u)\tan\chi - \rho} \quad \rightarrow \quad \tan\gamma \approx \frac{u}{\tan\chi - \rho} \qquad (4), (4_{abr.})$$

Applying the momentum transport theorem and neglecting much smaller terms, one may write

$$\frac{\partial}{\partial\theta}\left[\left(T - qv_b^2\right)\mathbf{i}_b\right] + \mathbf{F}'_w \cong 0 \qquad (5)$$

where $\mathbf{F}'_w$ is the resultant wall force per unit angle of contact, $q$ is the unit length belt mass and $qv_b^2$ is the momentum flux component in the belt direction, which is quite small in comparison with $T$ and is assumed constant along the belt path. Thus, the actual belt force $T$ and the elongation $\varepsilon$ may be replaced in the analysis by the "dynamic" force $\tilde{T} = T - qv_b^2$ and the "dynamical" elongation $\tilde{\varepsilon} = (T - qv_b^2)/S_{//}$.

Splitting the equilibrium condition (5) in the directions tangential and normal to the belt on the plane of rotation, indicating the transverse elasticity modulus with $E_z$, the elementary axial force with $dF_z$, the equivalent belt thickness and width with $h$ and $b$, introducing the belt elastic parameter $k = 2\tan\alpha\, S_\perp/S_{//}$, where $S_\perp = 2\tan\alpha E_z h r_\infty^2 / b$ [N] is a transverse stiffness parameter of the belt-pulley coupling, one gets

$$\tilde{\varepsilon}' = \tilde{\varepsilon}(1+\chi')\tan(\beta+\chi) \quad \rightarrow \quad \tilde{\varepsilon}' \approx \tilde{\varepsilon}\ \tan\beta \qquad (6), (6_{abr.})$$

$$\chi' = \frac{kx(1-x)(1-\tan\beta\tan\chi)}{\tilde{\varepsilon}\left(1-\dfrac{\tan\beta}{\cos^2\alpha\tan\gamma}\right)} - 1 \quad \rightarrow \quad kx \approx \tilde{\varepsilon}\left(1-\frac{\tan\beta}{\cos^2\alpha\tan\gamma}\right) \qquad (7), (7_{abr.})$$

$$dF_z = \frac{S_\perp x(1-x)}{\cos\chi}d\theta \quad \rightarrow \quad F'_z \approx S_\perp x \qquad (8), (8_{abr.})$$

where $\beta$, angle between the resultant elementary wall force and the radial direction, is given by

$$\tan\beta = \frac{f\sin\gamma}{f\cos\gamma + \tan\alpha\sqrt{1-\sin^2\alpha\sin^2\gamma}} \qquad (9)$$

Equation ($7_{abr.}$) leads to three relevant relationships, which will be recalled in the following:

for $\gamma \approx 0$, $\tilde{\varepsilon} \approx k_1 x$, where $k_1 = k\dfrac{\tan(\alpha+\arctan f)}{\tan\alpha}$

for $\gamma \approx \pm\pi/2$, $\tilde{\varepsilon} \approx kx$ (10 a,b,c)

for $\gamma \approx \pm\pi$, $\tilde{\varepsilon} \approx k_2 x$, where $k_2 = k\dfrac{\tan(\alpha-\arctan f)}{\tan\alpha}$ (< 0 usually)

We have thus four differential equations, Eqs. (1), (3), (6), (7), and one parametric equation, Eq. (4), in the five dependent variables $x$, $\tilde{\varepsilon}$, $\chi$, $u$ and $\gamma$, the first four of which are very small (<< 1), whilst the sliding angle $\gamma$ may range between $-\pi$ and $+\pi$: the mathematical consistency is then established.

The abridged relationships reported above on the right side ignore many small terms. Actually, the differential system appears of the "degenerescent" type, as it "degenerates" from the fourth to the third order when it is reduced to its abridged form (compare Eq. (7) and ($7_{abr.}$)) and not all the boundary conditions can be fulfilled. The problem is then of the "boundary layer" type and the variables change rather smoothly along almost the whole arc of contact but exhibit large gradients near the boundaries, in order to match the boundary conditions. The abridged model is then applicable in the inside of the wrap arc, while a complete analysis, valid as far as the contact boundaries, must necessarily use the full equations.

The full differential system may be solved only by numerical procedures, separately for each pulley, starting from one endpoint of the winding arc, where the vanishing of the transverse compression has to be imposed ($x = 0$) and proceeding towards the other endpoint, which is attained when the variable $x$ vanishes again. As three initial conditions must be specified, for $\varepsilon$, $\chi$, $u$ (or else $\gamma$), these three values are to be modified by trial and error by a sort of shooting technique until the three requested "external" conditions are fulfilled: wrap arc width, force ratio $T_{out} / T_{in}$ and axial thrust $F_z = \int_{wrap\ arc} dF_z$, calculable by Eq. (8).

It was proved in reference [8] that an adhesive region must be present in the inside of the contact region of the closing pulleys ($\rho > 0$), while a quasi-adhesive region settles in the opening pulleys ($\rho < 0$). All the previous relationships are valid in the adhesive region, but considering now $f$ as a variable adhesion factor $f_a \le f_s$, where $f_s$ is the coefficient of static friction, and $\gamma$ as the angle $\gamma_a$ of the resultant elementary adhesion force with the radial direction, whose values may be calculated by the equilibrium equations (6-7). The adherence limit is reached when $f_a = f_s$ and it was also proved in [8] that the upstream boundary of the adhesive region requires $f_a \ge f$ necessarily (i. e. $f_a = f$ if $f_s = f$).

As $\tan\chi = \rho$ = constant and $u = 0$ along the adhesive region, Equation (3) gives $\varepsilon' = 0$ (constant belt force), while Equation (1) gives, e. g. with reference to the upstream endpoint $U$ of the adhesive region,

$$x = 1-(1-x_U)\exp[-\rho(\theta-\theta_U)] \quad \rightarrow \quad x \cong x_U + \rho(\theta-\theta_U) \qquad (11), (11_{abr.})$$

so that the belt path has the shape of a logarithmic spiral, which, since $x$ and $\rho$ are very small, may be roughly confused with a linear spiral of Archimedes. Of course, the belt radius increases, at any fixed angular position, due to the pulley rotation, because $\rho > 0$.

## 3. CLOSED-FORM APPROXIMATIONS

Some typical features can be always identified in the diagrams of the numerical solutions. They are distinct for the four possible operation modes of the pulley, opening or closing, driver or driven, and permit constructing simple closed-form approximations for each mode, easier to handle for practical design purposes, by use of the abridged equations ($\ldots_{abr.}$) of the previous section.

### 3.1. Opening Pulley

**3.1.1. Quasi-adhesive regions.** In the opening pulley case ($\rho < 0$), a wide quasi-adhesive region settles inside the arc of contact, just downstream of a very short seating region. The last one is characterized by a radially inward sliding velocity ($\gamma \approx 0$), which yields the penetration $x_{in} \approx \tilde{\varepsilon}_{in}/k_1$ at the start of the main internal region by Eq. (10 a) (here, the subscripts *in* and *out* will refer to the main internal region endpoints, where $x \ne 0$, and not to the whole contact endpoints, where $x = 0$).

Moreover, the sliding angle $\gamma$ keeps quite small, negative and nearly constant along the quasi-adhesive region, while the gradients of the belt elongation $\tilde{\varepsilon}$ and of the radial penetration $x$ appear nearly constant and negative, so that the belt spirals outward in the motion direction.

Accounting for such remarks, the values of the above gradients can be calculated by the previous equations. Firstly, one derives $\tilde{\varepsilon}\,' \approx \rho - \tan\chi$ by Eqs. ($3_{abr.}$, $4_{abr.}$) and $\tilde{\varepsilon} \approx k_1 x$ by Eq. (10 a), and then, differentiating now the full equation (7), replacing the last results and accounting for the orders of magnitude of the variables, can obtain

$$\chi'' \approx \frac{\tan\chi}{x} - \frac{\tilde{\varepsilon}'}{\tilde{\varepsilon}} \approx \frac{1}{x}\left(\tan\chi - \frac{\rho - \tan\chi}{k_1}\right) \tag{12}$$

Since the plot of $\chi$ exhibits a local minimum in the quasi-adhesive region, where $\chi' = 0$ and $\chi'' > 0$, and is very flat in this region, also the second derivative $\chi''$ tends to vanish, as described in [4,8]. Therefore, Equation (12) permits writing $\tan\chi \approx \rho\,/\,(1 + k_1)$ and the searched gradients turn out to be

$$x' \approx \frac{\rho}{1+k_1} \qquad \tilde{\varepsilon}\,' \approx \frac{k_1\rho}{1+k_1} \tag{13 a,b}$$

Thus, moving ahead inside the quasi-adhesive region, one has, by Eqs. (13),

$$\tilde{\varepsilon} \approx \tilde{\varepsilon}_{in} + \frac{k_1\rho}{1+k_1}(\theta - \theta_{in}) \qquad x \approx \frac{\tilde{\varepsilon}_{in}}{k_1} + \frac{\rho}{1+k_1}(\theta - \theta_{in}) \tag{14 a,b}$$

As regards the main sliding region following the quasi-adhesive arc, where the torque is transmitted from/to the pulley to/from the belt, different approximate solutions are to be chosen for the driver or driven cases, here indicated with the subscripts $R$ and $N$ respectively.

**3.1.2. Driver pulley. Sliding region and axial thrust.** By inspection of several driver pulley solutions, it is observable that the sliding angle $\gamma$ is negative and its absolute value increases nearly proportionally to the angular distance from the point $O$ of virtual connection between the quasi-adhesive and sliding regions: $\chi(\theta) \approx \theta_O - \theta$. Replacing this expression into Eqs. (9) and ($6_{abr.}$) and neglecting the product $\sin^2\alpha \sin^2(\theta_O - \theta) << 1$, one gets the integrable form $d\tilde{\varepsilon}\,/\,\tilde{\varepsilon} \approx f \sin(\theta_O - \theta)\; d\theta\,/\,[f\cos(\theta_O - \theta) + \tan\alpha]$, yielding the cosine solution:

$$\tilde{\varepsilon} = \left[\tilde{\varepsilon}_{inR} + \frac{k_{1R}\rho_R}{1+k_{1R}}(\theta_O - \theta_{inR})\right]\left[\frac{f\cos(\theta_O - \theta) + \tan\alpha}{f + \tan\alpha}\right] \tag{15}$$

The radial penetration is obtainable by substitution of $\tilde{\varepsilon}$ into Eq. ($7_{abr.}$):

$$x = \left[\frac{\tilde{\varepsilon}_{inR}}{k_{1R}} + \frac{\rho_R}{1+k_{1R}}(\theta_O - \theta_{inR})\right]\left[\frac{1 - f\tan\alpha\cos(\theta_O - \theta)}{1 - f\tan\alpha}\right] \tag{16}$$

The angular boundary $\theta_O$ may be calculated in dependence on the entrance and exit values of the dynamical elongation, $\tilde{\varepsilon}_{inR}$ and $\tilde{\varepsilon}_{outR}$, by use of Eq. (15):

$$\tilde{\varepsilon}_{outR} = \left[\tilde{\varepsilon}_{inR} + \frac{k_{1R}\rho_R}{1+k_{1R}}(\theta_O - \theta_{inR})\right]\left[\frac{f\cos(\theta_O - \theta_{outR}) + \tan\alpha}{f + \tan\alpha}\right] =$$

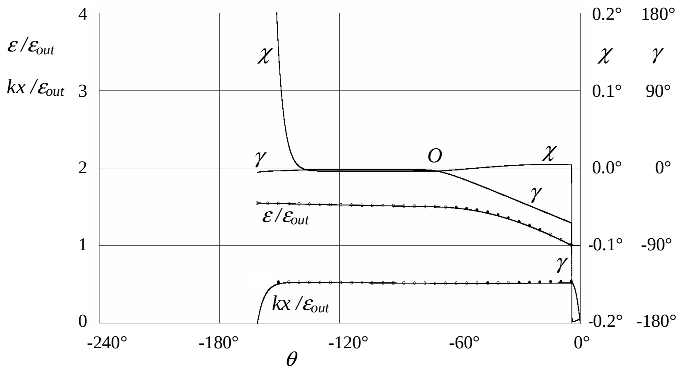


Figure 2. Opening driver pulley. Elongation $\varepsilon$, penetration $x$, inclination $\chi$, sliding angle $\gamma$, versus angular coordinate $\theta$. Data: $\alpha$ = 13°, $f$ = 0.35, $k$ =0.15, $\varepsilon_{out}$ = 0.001, $qv_b^2$ = 0.0001, $\rho$ = –0.0001. Dots: approximate solutions for $\varepsilon = \tilde{\varepsilon} + qv_b^2$ and $x$ by Eqs. (14-16)

$$= \tilde{\varepsilon}_{inR} - \frac{M_R}{r_R S_{//}} \tag{17}$$

where $M_R$ and $r_R$ are the driver torque and radius.

Then, integrating Eqs. (14 b) and (16) along the arc of contact, one gets the axial force $F_{zR}$

$$\frac{F_{zR}}{S_\perp} = \int_{\theta_{inR}}^{\theta_{outR}} x\,d\theta = \frac{\tilde{\varepsilon}_{inR}}{k_{1R}}(\theta_O - \theta_{inR}) + \left(\frac{\rho_R}{1+k_{1R}}\right)\frac{(\theta_O - \theta_{inR})^2}{2} +$$

$$\left[\frac{\tilde{\varepsilon}_{inR}}{k_{1R}} + \left(\frac{\rho_R}{1+k_{1R}}\right)(\theta_O - \theta_{inR})\right]\left[\frac{\theta_{outR} - \theta_O - f\tan\alpha\sin(\theta_{outR} - \theta_O)}{1 - f\tan\alpha}\right] -$$

$$I_{seat.} - I_{unseat.} \tag{18}$$

where $I_{seat.}$ and $I_{unseat.}$ are small corrections that take into consideration the decrease of the radial penetration in the seating and unseating region, which will be specified later on.

As observable in Fig. 2, the described approximate solutions are in good accordance with the numerical ones.

**3.1.2. Driven pulley. Sliding region and axial thrust.** The numerical solutions for the driven pulleys indicate a certain point $O$, located in practice at the beginning of the main sliding region, where $\tan\chi = \tan\gamma = x' = \tilde{\varepsilon}\,' = 0$, and point out also that $dx/d\tilde{\varepsilon}$ is nearly constant inside this region: $(x - x_O)\,/\,(\tilde{\varepsilon} - \tilde{\varepsilon}_O) \approx$ constant $= m$.

Solving Eq. ($7_{abr.}$) with respect to $\tan\gamma$ and observing that $\tilde{\varepsilon}\tan\beta = \cos^2\alpha\tan\gamma(\tilde{\varepsilon} - k_N x)$, it is possible to get like in [2]

$$\tan\gamma = \frac{\sqrt{(1 - f^2\tan^2\alpha)(k_{1N}x - \tilde{\varepsilon})(\tilde{\varepsilon} - k_{2N}x)}}{\cos\alpha(\tilde{\varepsilon} - k_N x)} \tag{19}$$

 

$$\tilde{\varepsilon}' = \cos\alpha\sqrt{\left(1-f^2\tan^2\alpha\right)\left(k_{1N}x-\tilde{\varepsilon}\right)\left(\tilde{\varepsilon}-k_{2N}x\right)} \qquad (20)$$

Moreover, integrating Eqs. ($1_{abr.}$, $3_{abr.}$), Equation ($4_{abr.}$) permits writing

$$x' = \rho_N + [\,\tilde{\varepsilon} - \tilde{\varepsilon}_O + x - x_O - \rho_N(\theta - \theta_O)]\,/\tan\gamma \qquad (21)$$

and, combining this result with Eqs. (19, 20), referring the subscript *out* to the end of the main sliding region and putting $R = \sqrt{\left(1-f^2\tan^2\alpha\right)\left(k_{1N}x_{outN}-\tilde{\varepsilon}_{outN}\right)\left(\tilde{\varepsilon}_{outN}-k_{2N}x_{outN}\right)}$, one may obtain

$$mR^2\cos\alpha = \rho_N R + [\,\tilde{\varepsilon}_{outN} - \tilde{\varepsilon}_O + x_{outN} - x_O - \rho_N(\theta_{outN} - \theta_O)](\,\tilde{\varepsilon}_{outN} - k_N\,x_{outN})\cos\alpha \qquad (22)$$

where $\tilde{\varepsilon}_O$ and $x_O$ can be obtained by Eqs. (14). As $x_{outN} = x_O + m(\tilde{\varepsilon}_{outN} - \tilde{\varepsilon}_O)$ by the previous assumption, Equation (22) permits a quick determination of the slope parameter $m$ by a few iterations, once $\theta_O$, $\tilde{\varepsilon}_{outN}$ and $\tilde{\varepsilon}_{inN}$ are fixed.

Replacing $x = x_O + m\,(\tilde{\varepsilon} - \tilde{\varepsilon}_O)$ into Eq. (20) and minding that $\tilde{\varepsilon}_O = k_{1N}\,x_O$ by Eq. (10 a) or (19), as $\tan\gamma_O = 0$, an integrable expression is obtainable:

$$\tilde{\varepsilon}' = \cos\alpha\sqrt{\left(1-f^2\tan^2\alpha\right)}\times \sqrt{\left(mk_{1N}-1\right)\left(\tilde{\varepsilon}-\tilde{\varepsilon}_O\right)\left[\left(1-mk_{2N}\right)\left(\tilde{\varepsilon}-\tilde{\varepsilon}_O\right)+\tilde{\varepsilon}_O\left(1-\frac{k_{2N}}{k_{1N}}\right)\right]} \qquad (23)$$

which yields the hyperbolic cosine solution

$$\tilde{\varepsilon} = \left[\tilde{\varepsilon}_{inN} + \frac{k_{1N}\rho_N}{1+k_{1N}}\left(\theta_O-\theta_{inN}\right)\right]\times \left\{1+\frac{\left(k_{1N}-k_{2N}\right)}{2k_{1N}\left(1-mk_{2N}\right)}\left[\cosh\Omega\left(\theta-\theta_O\right)-1\right]\right\} \qquad (24)$$

$$x = \left[\frac{\tilde{\varepsilon}_{inN}}{k_{1N}} + \frac{\rho_N}{1+k_{1N}}\left(\theta_O-\theta_{inN}\right)\right]\times \left\{1+\frac{m\left(k_{1N}-k_{2N}\right)}{2\left(1-mk_{2N}\right)}\left[\cosh\Omega\left(\theta-\theta_O\right)-1\right]\right\} \qquad (25)$$

where

$$\Omega = \cos\alpha\sqrt{\left(1-f^2\tan^2\alpha\right)\left(mk_{1N}-1\right)\left(1-mk_{2N}\right)} \qquad (26)$$

The solution (24-26) is similar to reference [14], which however dealt with a steady drive.

The angular boundary $\theta_O$ may be calculated in dependence on the entrance and exit values of the dynamical elongation using Eq. (24):

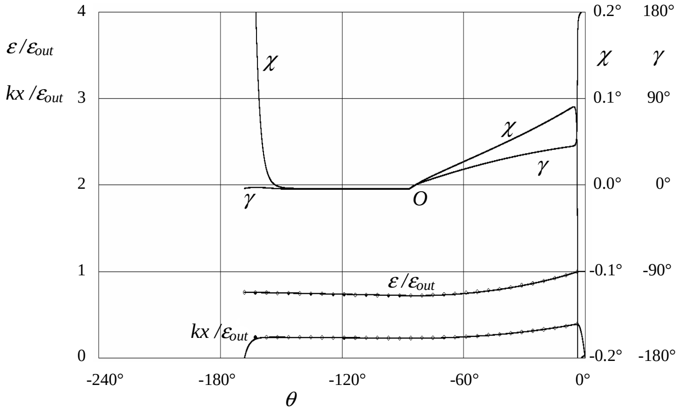


Figure 3. Opening driven pulley. Elongation $\varepsilon$, penetration $x$, inclination $\chi$, sliding angle $\gamma$, versus angular coordinate $\theta$. Data: $\alpha$ = 13°, $f$ = 0.35, $k$ = 0.15, $\varepsilon_{out}$ = 0.001, $qv_b^2$ = 0.0001, $\rho$ = –0.0001. Dots: approximate solutions for $\varepsilon = \tilde{\varepsilon} + qv_b^2$ and $x$ by Eqs. (14, 24-25)

$$\tilde{\varepsilon}_{outN} = \left[\tilde{\varepsilon}_{inN} + \frac{k_{1N}\rho_N}{1+k_{1N}}\left(\theta_O-\theta_{inN}\right)\right]\times \left\{1+\frac{\left(k_{1N}-k_{2N}\right)}{2k_{1N}\left(1-mk_{2N}\right)}\left[\cosh\Omega\left(\theta_{outN}-\theta_O\right)-1\right]\right\} = \tilde{\varepsilon}_{inN} + \frac{M_N}{r_N S_{//}} \qquad (27)$$

where $M_N$ and $r_N$ are the driven torque and radius.

The axial thrust can be obtained at last by the integration of Eq. ($8_{abr.}$)

$$\frac{F_{zN}}{S_\perp} = \int_{\theta_{inN}}^{\theta_{outN}} x\,d\theta = \frac{\tilde{\varepsilon}_{inN}}{k_{1N}}\left(\theta_O-\theta_{inN}\right) + \left(\frac{\rho_N}{1+k_{1N}}\right)\frac{\left(\theta_O-\theta_{inN}\right)^2}{2} + \left[\frac{\tilde{\varepsilon}_{inN}}{k_{1N}} + \left(\frac{\rho_N}{1+k_{1N}}\right)\left(\theta_O-\theta_{inN}\right)\right]\left\{\theta_{outN}-\theta_O + \frac{m\left(k_{1N}-k_{2N}\right)}{2\left(1-mk_{2N}\right)}\left(\frac{\sinh\Omega\left(\theta_{outN}-\theta_O\right)}{\Omega}-\theta_{outN}+\theta_O\right)\right\} - I_{seat.} - I_{unseat.} \qquad (28)$$

where $I_{seat.}$ and $I_{unseat.}$ have the same meaning of the driver case, to be specified later on.

Figure 3 indicates a good accordance between the solutions of the full equations and the above approximations also for this case.

### 3.2. Closing Pulley

**3.2.1. Adhesive regions.** As mentioned in the previous section, the closing pulleys exhibit a large adhesive region inside the arc of contact, where the belt force and the belt angle are constant, $\tilde{\varepsilon}' = 0$, $\tan\chi = \rho > 0$, so that the belt spirals altogether inward in the rotation direction. This region is immediately downstream of a short seating region, where the sliding velocity is nearly radial and inward directed ($\gamma \approx 0$), so that, at the entrance of the adhesive region, the radial penetration is $x_U \approx \tilde{\varepsilon}_{in}/k_1$ by Eq. (10 a) and, moving ahead inside this region, one has by Eq. ($11_{abr.}$)

$$\tilde{\varepsilon} = \tilde{\varepsilon}_{in} \qquad x \cong \frac{\tilde{\varepsilon}_{in}}{k_1} + \rho(\theta - \theta_{in}) \tag{29}$$

It was also shown in [8] that all the variables are continuous at the downstream boundary $D$ of the adhesive region save $\gamma$, which is subject to a certain jump $\Delta\gamma$. The downstream value $\gamma_D$ can be calculated by the equilibrium equation ($7_{abr.}$) normal to the belt, in dependence on the elastic variables $\tilde{\varepsilon}_D = \tilde{\varepsilon}_{in}$ and $x_D = \tilde{\varepsilon}_{in}/k_1 + \rho(\theta_D - \theta_{in})$:

$$\tan\gamma_D = \pm\sqrt{\left[\frac{f\left(kx_D + \tilde{\varepsilon}_D \tan^2\alpha\right)}{\sin\alpha\left(\tilde{\varepsilon}_D - kx_D\right)}\right]^2 - \frac{1}{\cos^2\alpha}} \tag{30}$$

When choosing the sign of (30), one has to mind that $\gamma_D$ is always in the first quadrant in the driven case, while in the driver case, $\gamma_D$ is in the fourth or third quadrant for $\tilde{\varepsilon}_D > kx_D$ or $\tilde{\varepsilon}_D < kx_D$ respectively (see Eq. ($7_{abr.}$)).

**3.2.2. Driver pulley. Sliding region and axial thrust.** The sliding angle $\gamma$ is negative and its magnitude increases nearly proportionally to the angular distance from the starting point $D$ of the sliding region: $\gamma(\theta) \approx \gamma_D - (\theta - \theta_D)$. Replacing this expression into Eq. (9), replacing then $\tan\beta$ into the tangential equilibrium equation ($6_{abr.}$) and neglecting the product $\sin^2\alpha \sin^2(\gamma_D + \theta_D - \theta)$ with respect to the unity, one gets the integrable form $d\tilde{\varepsilon}/\tilde{\varepsilon} \approx f\sin(\gamma_D + \theta_D - \theta)\, d\theta/[f\cos(\gamma_D + \theta_D - \theta) + \tan\alpha]$, giving the cosine solution:

$$\tilde{\varepsilon} = \tilde{\varepsilon}_{inR}\frac{f\cos(\gamma_D + \theta_D - \theta) + \tan\alpha}{f\cos\gamma_D + \tan\alpha} \tag{31}$$

The radial penetration is obtainable by substitution of $\tilde{\varepsilon}$ into the equilibrium equation normal to the belt ($7_{abr.}$)

$$x = \left(\frac{\tilde{\varepsilon}_{inR}\tan\alpha}{k_R}\right)\left[\frac{1 - f\tan\alpha\cos(\gamma_D + \theta_D - \theta)}{\tan\alpha + f\cos\gamma_D}\right] \tag{32}$$

The quantities $x_D$ and $\gamma_D$ are functions of the unknown internal boundary $\theta_D$, which may be calculated in dependence on the entrance and exit values of the dynamical elongation, $\tilde{\varepsilon}_{inR}$ and $\tilde{\varepsilon}_{outR}$, putting $\tilde{\varepsilon} = \tilde{\varepsilon}_{outR}$ and $\theta = \theta_{outR}$ into Eq. (31):

$$\tilde{\varepsilon}_{outR} = \tilde{\varepsilon}_{inR}\left[\frac{f\cos(\gamma_D + \theta_D - \theta_{outR}) + \tan\alpha}{f\cos\gamma_D + \tan\alpha}\right] = \tilde{\varepsilon}_{inR} - \frac{M_R}{r_R S_{//}} \tag{33}$$

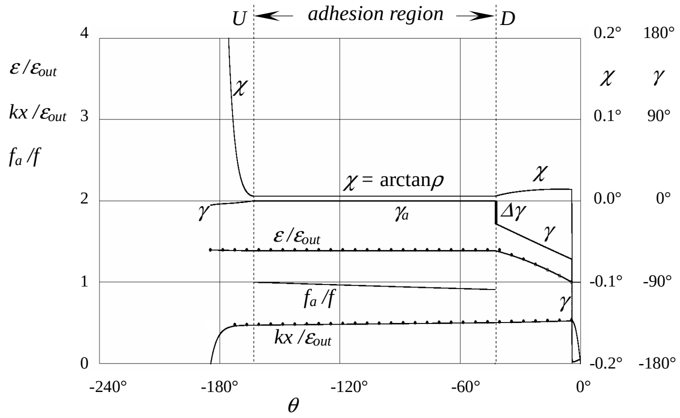


Figure 4. Closing driver pulley. Elongation $\varepsilon$, penetration $x$, inclination $\chi$, sliding angle $\gamma$, adhesion factor $f_a$ ($f_s = f$), versus angular coordinate $\theta$. Data: $\alpha = 13°$, $f = 0.35$, $k = 0.15$, $\varepsilon_{out} = 0.001$, $qv_b^2 = 0.0001$, $\rho = 0.0001$. Dots: approximate solutions for $\varepsilon = \tilde{\varepsilon} + qv_b^2$ and $x$ by Eqs. (29-30, 31-32)

Integrating Eq. ($8_{abr.}$) along the whole arc of contact, one gets the axial force $F_{zR}$

$$\frac{F_{zR}}{S_\perp} = \int_{\theta_{inR}}^{\theta_{outR}} x\,d\theta = \frac{\tilde{\varepsilon}_{inR}}{k_{1R}}\left(\theta_D - \theta_{inR}\right) + \rho_R\frac{\left(\theta_D - \theta_{inR}\right)^2}{2} +$$
$$+ \frac{\tilde{\varepsilon}_{inR}\tan\alpha}{k_R\left(\tan\alpha + f\cos\gamma_D\right)}\left\{\theta_{outR} - \theta_D + \right. \tag{34}$$
$$\left. + f\tan\alpha\left[\sin\left(\gamma_D + \theta_D - \theta_{outR}\right) - \sin\gamma_D\right]\right\} - I_{seat.} - I_{unseat.}$$

where $I_{seat.}$ and $I_{unseat.}$ are similar to the previous cases.

Figure 4 compares the numerical solution and the above approximations for the present mode and a very fine agreement can be observed between the diagrams.

**3.2.3. Driven pulley. Sliding region and axial thrust.** Similarly to the opening pulleys, the numerical solutions for the closing driven pulleys indicate a nearly linear relationship between $x$ and $\tilde{\varepsilon}$ inside the main sliding region, $dx/d\tilde{\varepsilon} \approx$ constant $= m$, save some small deviation near the starting point $D$. Therefore, relationships similar to Eqs. (19-22) may be used, save the replacement of the subscript $O$ with $D$, where $\tilde{\varepsilon}_D = \tilde{\varepsilon}_{inN}$ and $x_D \cong \tilde{\varepsilon}_{inN}/k_{1N} + \rho_N\left(\theta_D - \theta_{inN}\right)$.

As the linear relationship between $\tilde{\varepsilon}$ and $x$ may be prolonged as far as a virtual initial point ($\tilde{\varepsilon}_D/k_{1N}$, $\tilde{\varepsilon}_D$) of the sliding region with a good approximation, compensating the small deviation mentioned above, it is possible to write $x_{out} = \tilde{\varepsilon}_{inN}/k_{1N} + m\,(\tilde{\varepsilon}_{outN} - \tilde{\varepsilon}_{inN})$ and Equation (22) leads to a quick determination of the slope parameter $m$ by a few iterations, once $\theta_D$, $\tilde{\varepsilon}_{outN}$ and $\tilde{\varepsilon}_{inN}$ are fixed.

The subsequent procedure is quite similar to the opening pulley case, save replacing $x = \tilde{\varepsilon}_{inN}/k_{1N} + m\,(\tilde{\varepsilon} - \tilde{\varepsilon}_{inN})$ into Eq. (20), and yields similar results

$$\tilde{\varepsilon} = \tilde{\varepsilon}_{inN}\left\{1 + \frac{(k_{1N} - k_{2N})}{2k_{1N}(1 - mk_{2N})}\left[\cosh \Omega(\theta - \theta_D) - 1\right]\right\} \tag{35}$$

$$x = \frac{\tilde{\varepsilon}_{inN}}{k_{1N}}\left\{1 + \frac{m(k_{1N} - k_{2N})}{2(1 - mk_{2N})}\left[\cosh \Omega(\theta - \theta_D) - 1\right]\right\} \tag{36}$$

Despite the small discontinuity of $x$ at point $D$, the overall fit with the numerical diagrams is quite satisfactory.

The angular boundary $\theta_D$ may be calculated using Eq. (35):

$$\tilde{\varepsilon}_{outN} = \tilde{\varepsilon}_{inN}\left\{1 + \frac{(k_{1N} - k_{2N})}{2k_{1N}(1 - mk_{2N})}\left[\cosh \Omega(\theta_{outN} - \theta_D) - 1\right]\right\} = $$

$$= \tilde{\varepsilon}_{inN} + \frac{M_N}{r_N S_{//}} \tag{37}$$

and the axial thrust can be obtained at last by the integration of Eq. ($8_{abr.}$)

$$\frac{F_{zN}}{S_\perp} = \int_{\theta_{inN}}^{\theta_{outN}} x\, d\theta = \frac{\tilde{\varepsilon}_{inN}}{k_{1N}}(\theta_D - \theta_{inN}) + \rho_N \frac{(\theta_D - \theta_{inN})^2}{2} +$$

$$+ \frac{\tilde{\varepsilon}_{inN}}{k_{1N}}\left\{\theta_{outN} - \theta_D + \right. \tag{38}$$

$$\left. + \frac{m(k_{1N} - k_{2N})}{2(1 - mk_{2N})}\left[\frac{\sinh \Omega(\theta_{outN} - \theta_D)}{\Omega} - \theta_{outN} + \theta_D\right]\right\} - I_{seat.} - I_{unseat}$$

Also the above approximations give a very good fit, as observable in Fig. 5.

### 3.3. Seating and Unseating Regions

The simplified analysis described so far ignores the short seating and unseating regions, where the belt transverse compression $x$ decreases until vanishing at the outer ends of the wrap arc.

Reference [15] shows that the elastic belt arching in the free span is negligible for V-belts, due to the gradual penetration of the belt into the groove, which flattens the bending line, so that there is very little difference with the circular-straight path of a perfectly flexible belt. Nevertheless, as the steady model of [5] does not apply to transient conditions, the boundary analysis of [4] will here be used and the conventional bending effect will be included.

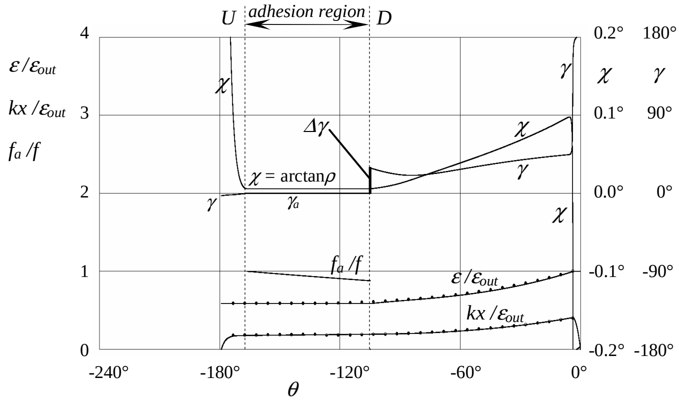


Figure 5. Closing driven pulley. Elongation $\varepsilon$, penetration $x$, inclination $\chi$, sliding angle $\gamma$, adhesion factor $f_a$ ($f_s = f$), versus angular coordinate $\theta$. Data: $\alpha$ = 13°, $f$ = 0.35, $k$ = 0.15, $\varepsilon_{out}$ = 0.001, $qv_b^2$ = 0.0001, $\rho$ = 0.0001. Dots: approximate solutions for $\varepsilon = \tilde{\varepsilon} + qv_b^2$ and $x$ by Eqs. (29-30, 35-36)

Assuming that the sliding direction is nearly radial ($\gamma \approx 0$ in the seating region and $\gamma \approx \pi$ in the unseating one) and replacing $\chi'$ with $x''$, Equation ($7_{abr.}$) gives rise to two second order differential equations, for the entrance and exit regions:

$$x'' - \frac{k_{seat.,unseat.}}{\tilde{\varepsilon}_{in,out}}\, x = -1 \tag{39}$$

These equations are valid for opening or closing, driver or driven pulleys and accounting for Eqs. (10 a,c), one has to put $k_{seat.} = k_1 > 0$ and $k_{unseat.} = k_2 < 0$ ($k_2$ is negative as generally $f > \tan\alpha$ for rubber belt variators). Therefore, hyperbolic or trigonometric solutions arise in the two cases. The two integration constants may be determined imposing $x = 0$ at the outer end of the contact and $x = x_{in,out}$ at an "artificial" inner connection point with the main contact region. Thus, a new unknown arises, i. e. the angular extent $\Delta\theta_b$ of the boundary region, which can be calculated however by simply imposing the vanishing of the gradient $x'$ at the inner end, where the gradient ceases indeed to be large. Then

$$x_{seating} = x_{in}\left[1 - e^{-\sqrt{\frac{k_1}{\tilde{\varepsilon}_{in}}}(\theta - \theta_{in})}\right] = \frac{\tilde{\varepsilon}_{in}}{k_1}\left[1 - e^{-\sqrt{\frac{k_1}{\tilde{\varepsilon}_{in}}}(\theta - \theta_{in})}\right] \tag{40}$$

$$x_{unseating} = \left(-\frac{\tilde{\varepsilon}_{out}}{k_2}\right)\left[\cos\left(\sqrt{-\frac{k_2}{\tilde{\varepsilon}_{out}}}(\theta_{out} - \theta)\right) - 1 + \right.$$

$$\left. + \left[\sqrt{\left(1 - \frac{x_{out}k_2}{\tilde{\varepsilon}_{out}}\right)^2 - 1}\right]\sin\left(\sqrt{-\frac{k_2}{\tilde{\varepsilon}_{out}}}(\theta_{out} - \theta)\right)\right] \tag{41}$$

As the coefficients $\sqrt{|k_{1,2}|/\varepsilon_{in,out}}$ of the independent variable $\theta$ are very large, the variable $x$ changes very rapidly. Moreover, the unseating angular width is $\Delta\theta_{unseat.}$ = $\sqrt{-\tilde{\varepsilon}_{out}/k_2}\,\arctan\sqrt{\left(1-x_{out}k_2/\tilde{\varepsilon}_{out}\right)^2-1}$, while the seating region width $\Delta\theta_{seat.}$ appears to diverge, but the exponential decay is quite sharp all the same, with a rapid asymptotic matching with the inner region.

Summarizing, the integrals of Eqs. (18), (28), (34), (38) can be corrected, for the sake of a greater precision, subtracting the axial thrust losses in the boundary regions:

$$\frac{\Delta F_{z,seating}}{S_\perp}=I_{seating}=\int_{\theta_{in}}^{\infty}\left(x_{in}-x_{seating}\right)d\theta=\left(\frac{\tilde{\varepsilon}_{in}}{k_1}\right)^{3/2} \tag{42}$$

$$\frac{\Delta F_{z,unseating}}{S_\perp}=I_{unseating}=\int_{\theta_{out}-\Delta\theta_{unseating}}^{\theta_{out}}\left(x_{out}-x_{unseating}\right)d\theta=$$
$$=\left(x_{out}-\frac{\tilde{\varepsilon}_{out}}{k_2}\right)\Delta\theta_{unseating}-\left(-\frac{\tilde{\varepsilon}_{out}}{k_2}\right)^{3/2}\sqrt{\left(1-\frac{x_{out}k_2}{\tilde{\varepsilon}_{out}}\right)^2-1} \tag{43}$$

## 4. EXPERIMENTATION

Some experimental tests were carried out on a continuously variable transmission (CVT) using the test bench of Fig. 6, which was widely described in [13-14].

A DC electric motor drove the transmission, while a pneumatically operated disk brake applied the resistant torque. The continuously variable unit consisted in a small power motorcycle variator with a downstream reduction gearing of ratio 13:1 and a centrifugal clutch, which was blocked during the tests. Another gear coupling was connected upstream of the variator, stepping up the speed with a ratio reciprocal of the downstream gears, in order to avoid too high speeds of the driving motor.

The speed and torque were measured on the driver and driven sides by means of two speed-torque meters of the strain-gauge type and the winding radius changes of both pulleys were measured by two LASER sensors.

The electric signals were channelled to a data acquisition system and worked out by a special software. The data were processed by a low-pass Butterworth filter of the first order with phase lag retrieval, whose cut-off frequency was equal to the fundamental harmonic, determined by FFT.

The belt stiffness in the longitudinal and transverse directions was measured on a material testing machine for tensile/compression measurements, obtaining the values, $S_{//}$ = 59000 N, $S_\perp$ = 15000 N (for speed ratio 1:1). Load tests on a clamped piece of belt gave the flexural stiffness $S_f$ = 6500 Nmm

The experimental evaluation of the axial thrust was indirect, as it was calculated using the measures of the wrap radii and the knowledge of the operative characteristics of the two actuators (see Fig. 7).

On the driver side, a centrifugal mass system adjusted the speed ratio to the input speed. The geometrical shape of the centrifugal mass tracks had been detected optically with a great accuracy, as reported in [13], and permitted correlating the driver axial thrust with the axial position of the movable half-pulley, i. e. with the belt winding radius, by use of the principle of virtual work,

$$F_{zR}\cong\frac{M\omega_R^2 r_M}{2\tan\alpha}\frac{dr_M}{dr_R} \tag{44}$$

where $M$ is the total centrifugal mass, $r_M$ indicates its radial position and $dr_M/dr_R$ was calculated in dependence of the profile of the centrifugal ramp.

On the driven pulley, a loading spring generated the belt forcing and moreover, the axial thrust was corrected by the

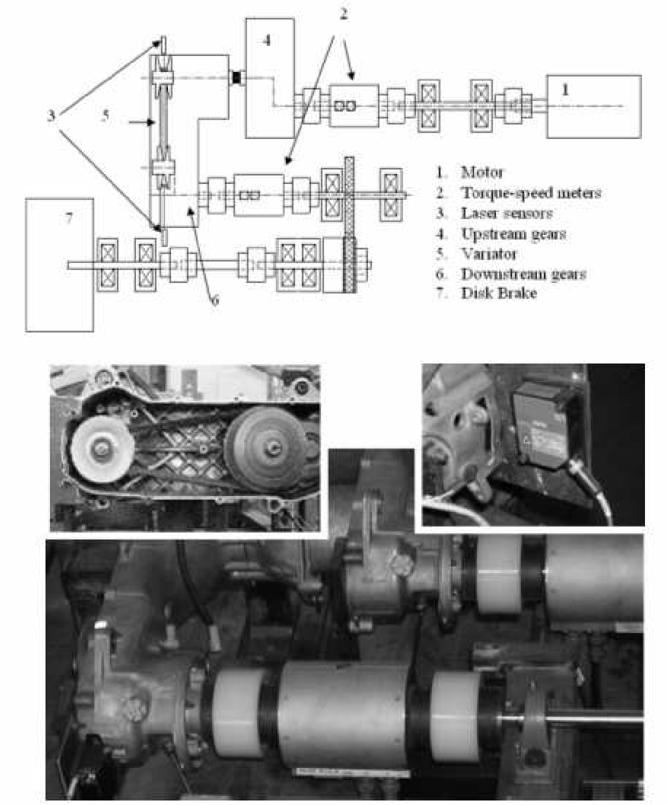


Figure 6. Experimental test bench.

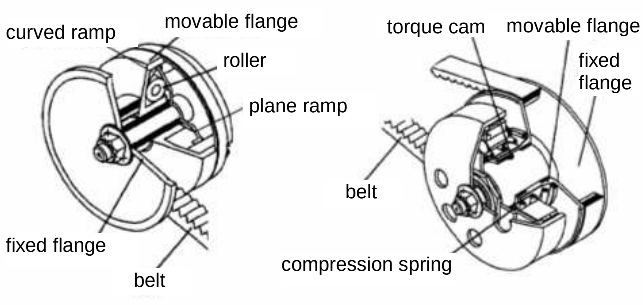


Figure 7. Driver and driven actuators

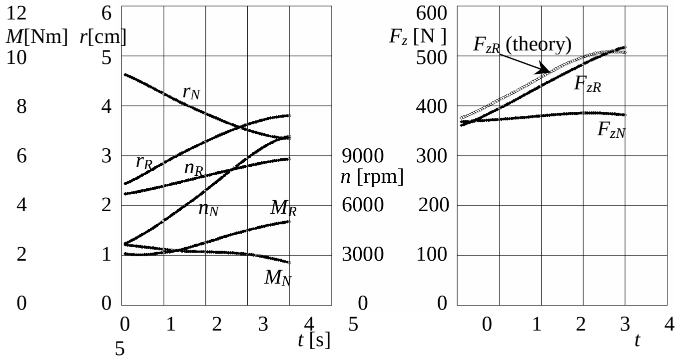


Figure 8. Shift up test. Data: $\alpha = 13°$, $f = 0.4$, $S_l = 59000$ N, $S_\perp = 15000$ N (for $\omega_N/\omega_R = 1$)

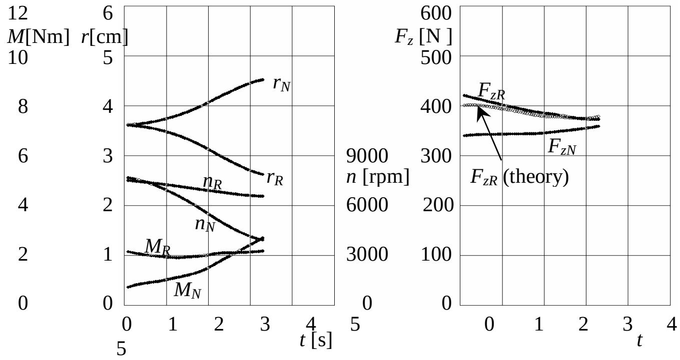


Figure 9. Shift down test. Data: $\alpha = 13°$, $f = 0.4$, $S_l = 59000$ N, $S_\perp = 15000$ N (for $\omega_N/\omega_R = 1$)

resistant torque through a suitable helical shape of the coupling tracks between the movable and fixed half-pulleys. The total axial thrust was [13]:

$$F_{zN} \cong F_0 + K\left(-2\Delta r_N \tan\alpha\right) + \frac{2M_{mov.N}}{d}\tan\delta_h \tag{45}$$

where $F_0$ is the pre-load in the fully closed configuration of the half-pulleys, $K$ the spring stiffness, $-2\Delta r_N \tan\alpha$ (> 0) the additional spring compression deflection, $\delta_h$ and $d$ the helix angle and diameter and $M_{mov.N}$ the driven torque fraction absorbed by the guide of the movable half-pulley.

Table 1 reports the data of the characteristic parameters of the CVT.

The efficiency losses and the moments of inertia of the CVT were evaluated running the pulleys without the belt and then, the measured torque on the input shaft was curtailed of the torque lost in the upstream gears and of the inertia torque, while the output shaft torque was raised likewise due to the downstream power losses and inertia.

Shift tests were performed on the described test bench, for various resistant torques and shift speeds, and all the variables were measured for each pulley at regularly spaced time instants.

Starting from the experimental evaluation of the axial forces $F_{zR}$ and $F_{zN}$, one of them was chosen as an entry for the theoretical model, and to be precise the axial thrust on the driven side, and the calculation was developed using the previous analytical model as far as evaluating the other axial force, on the driver side, in order to compare with the experimental result.

In practice, the two unknowns, $\tilde{\varepsilon}_{inN}$ , "dynamical" elongation in the slack strand, and $\theta_D$ or $\theta_O$ angular coordinate of the boundary point separating the adhesive or quasi-adhesive region from the main sliding region, were changed by a systematic trial and error procedure, until the torque and thrust equations were satisfied with an acceptable accordance with the experimental data.

Then, knowing the elongation entries, $\tilde{\varepsilon}_{inR} = \tilde{\varepsilon}_{outN}$ and $\tilde{\varepsilon}_{outR} = \tilde{\varepsilon}_{inN}$ , for the driver pulley, the angular coordinate of the starting point of the sliding region was calculated by trial and error, until the torque equation was fulfilled by the experimental torque datum. Finally, the theoretical axial thrust on the driver side was calculated, in practice in dependence on the driven axial thrust, and was compared with its experimental counterpart.

Figures 8 and 9 show examples of the experimental diagrams of the radii, speeds, torques and axial forces during a shift up and a shift down phase. The driver theoretical axial thrust is reported in the figures and a fine agreement can be clearly observed between the theory and the experiments

| | |
|---|---|
| belt length | 758 mm |
| centre distance | 255 mm |
| belt width | 15.5 mm |
| unit length mass of belt | 0.124 g/mm |
| longitudinal stiffness | $S_{//}$ = 59000 N |
| axial stiffness (for speed ratio 1:1) | $S_\perp$ = 15000 N |
| groove angle | 13 deg |
| belt-pulley coefficient of friction | 0.4 |
| total centrifugal mass (primary actuator) | 42.6 g |
| spring stiffness (secondary actuator) | 4.9 N/mm |
| axial pre-load (secondary actuator) | 275 N |
| angle of helical guide | 41 deg |

Table 1. Variator data

.

## 5. CONCLUSION

The present analysis starts from a complete mathematical model for the mechanical behavior of the rubber belt variators during the ratio shift, which is based on a new formulation of the mass conservation condition, imposing the balance of the mass increase inside a fixed elementary control volume and the mass flux through its control surface. By a careful examination of many complete numerical solutions, a set of easily calculable closed-form approximations is constructed, applicable to a large variety of different cases, of opening or closing, driver or driven pulleys, with the aim at providing a quick tool for the design and the analysis of the rubber belt CVT's.

The approximate solutions show a very good matching with the numerical solutions of the full model and may be also conveniently applied to compare the theory with the experimental results. For this purpose, several shift phases, more or less rapid, were carried out on a small rubber belt variator mounted on a test bench. Series of measures of the wrap radii and of the torque and the speed on the driving and driven shafts were taken at equally spaced time instants and collected to be worked out. The axial thrust on the one and the other pulley was measured in an indirect way, using the instant wrap radii and the knowledge of the operative characteristics of the actuators. The correspondence of the axial thrust, such as calculable by the theory and as given by the experiments, turns out to be acceptable, which may be retained as a validation of the approximate model.

## REFERENCES


[1] Dolan, J.P., and Worley, W.S., 1985, "Closed-Form Approximations to the Solutions of V-Belt Force and Slip Equations," *ASME J. of Mech., Transm. and Autom. in Design*, **107**, pp. 292-300.

[2] Sorge, F., 1996, "A Qualitative-Quantitative Approach to V-Belt Mechanics," *ASME J. of Mech. Design*, **118**, pp. 15-21.

[3] Gerbert, G., 1999, *Traction Belt Mechanics*, Chalmers University of Technology, Göteborg, Sweden.

[4] Gerbert, G., and Sorge, F., 2002, "Full Sliding "Adhesive-Like" Contact of V-Belts," *ASME J. of Mech. Design*, **124**, pp. 706-712.

[5] Kong, L., and Parker, R.G., 2006, "Mechanics and Sliding Friction in Belt Drives with Pulley Grooves," *ASME J. of Mech. Design*, **128**, pp. 494-502.

[6] Sorge, F., 2004, "Analysis of the Ratio Shift Transient in V-Belt Variators," *11th IFToMM World Congress in Mechanism and Machine Science*, Tianjin, China.

[7] Sorge, F., 2004, "Transient Mechanics of V-Belt Variators," *CVT '04*, Davis CA, USA.

[8] Sorge, F., 2008, "A Theoretical Approach to the Shift Mechanics of Rubber Belt Variators", *ASME J. of Mech. Des.*, (2008), **130**, pp. 122602-(1-9), DOI: 10.1115/1.2991140.

[9] Ide, T., Hirokazu, U., and Kataoka, R., 1996, "Experimental investigation on shift speed characteristics of a metal V-belt CVT", *JSAE Paper n. 9636330, CVT '96*, Yokohama, Japan.

[10] Carbone, G., Mangialardi, L., and Mantriota, G., 2005, "The Influence of Pulley Deformation on the Shifting Mechanism of Metal Belt CVT," *ASME J. of Mech. Design*, **127**, pp. 103-113.

[11] Sorge, F., 2007, "Shift Mechanics of Metal Belt CVT," *JSAE Paper n. 20074542, CVT Hybrid 2007,* Yokohama, Japan.

[12] Sorge, F., Beccari, A., and Cammalleri, M., 2001, "Operative Variator Characterization for CVT Improvement", *The JSME Intern. Confer. on Motion and Power Transmissions*, (2001), Fukuoka, Japan.

[13] Cammalleri, M., 2005, "A new approach to the design of a speed-torque controlled rubber V-belt variator", *Proc. of the IMechE, part D, J. of Automobile Engineering*, **219**, n. 12, pp. 1413-1428.

[14] Cammalleri, M., Conti, A., and Sorge, F., 2007, "Experimental Results for a Rubber Belt Variator in Shift Condition", *XVIII Congr. AIMETA*, Brescia, Italy, (CD).

[15] Sorge, F., 2009, "Joint Influence of Transverse Compression and Shear-Flexural Stiffness on Rubber V-Belt Mechanics", *The JSME Intern. Confer. on Motion and Power Transmissions*, MPT2009, May 13-15, 2009, Sendai, Japan.